We are IntechOpen, the world's leading publisher of Open Access books
Built by scientists, for scientists

6,900
Open access books available

186,000
International authors and editors

200M
Downloads

Our authors are among the

154
Countries delivered to

TOP 1%
most cited scientists

12.2%
Contributors from top 500 universities

CLARIVATE ANALYTICS
BOOK CITATION INDEX
INDEXED

WEB OF SCIENCE™

Selection of our books indexed in the Book Citation Index in Web of Science™ Core Collection (BKCI)

Interested in publishing with us?
Contact book.department@intechopen.com

Numbers displayed above are based on latest data collected.
For more information visit www.intechopen.com

12

Protein-Noble Gas Interactions Investigated by Crystallography on Three Enzymes - Implication on Anesthesia and Neuroprotection Mechanisms

Nathalie Colloc'h[1], Guillaume Marassio[1] and Thierry Prangé[2]
[1]*CI-NAPS UMR 6232 Université de Caen Basse-Normandie – CNRS, Centre Cyceron, Caen,*
[2]*LCRB, UMR 8015 – CNRS – Université Paris Descartes, Faculté de Pharmacie, Paris, France*

1. Introduction

General anesthetics have been used in clinical practice since the middle of the XIXth century, but their molecular mechanisms of action on the nervous system remains poorly understood. The main targets of most inhalational anesthetic are pentameric ligand-gated ion channels such as inhibitory $GABA_A$ (γ-amino-butyric acid) receptors whose activity is potentiated by general anesthetics. However, the main targets of gaseous anesthetics like xenon or nitrous oxide are excitatory NMDA (N-methyl-D-aspartate) receptors and nicotinic acetylcholine receptors whose activity is inhibited by gaseous anesthetics (Campagna et al., 2003; Franks, 2008). The use of gaseous anesthetics became widely applicable in the nineteen-fifties, nitrous oxide being often administrated in complement of halogenated anesthetics. Xenon anesthetic properties have been described by Cullen in 1951 (Cullen et al., 1951), and is used in anesthesia since mid-2000 (Sanders et al., 2004; Sanders et al., 2005) in spite of its excessive cost, a major obstacle to its widespread use (Kennedy et al., 1992).

Anesthesia is a complex process that refers to several physiologically altered functions. Early stages of anesthesia such as amnesia and hypnosis required anesthetic concentrations lower than those required to produce deep sedation and reduction of motor and automomic responses to noxious stimuli (Campagna et al., 2003). Scales that assess the *in-vivo* potency of inhaled anesthetics in humans are based on the minimum alveolar anesthetic concentrations (MAC) that are associated with well-defined behavioural endpoints. Following this, MAC-awake defines the MAC that induces the first stages of anesthesia such as amnesia and hypnosis, and MAC-immobility defines the MAC that produces deep sedation and suppresses movement in response to a noxious stimuli.

Anesthesia mechanisms were for a long time though to be mediated by non-specific membranous perturbation (Trudell, 1977). This membranous theory was based on the Meyer-Overton rule that showed an almost perfect relationship between the anesthetic property of a chemical compound and its solubility in olive oil or benzene. However, more and more exceptions were found to the Meyer-Overton rule such as the non-immobilizers

predicted to be potent anesthetics which indeed produced amnesia but not anesthesia or the eniantomers which have the same solubility in lipids but different anesthetic potencies (Campagna et al., 2003). Since the mid-1980, general anesthetics are though to act by disrupting protein functions (Franks et al., 1984; Franks et al., 1994). Chemical compounds that cross the blood brain barrier are generally soluble in lipids and could explain the Meyer-Overton rule (Franks, 2008). Anesthetics act mainly at ionotropic receptors which play a key role in regulation of ions' concentration on each side on the cytoplasmic membrane (Campagna et al., 2003). For a review of the major targets of general anesthetics and their effects, see (Yamakura et al., 2000).

Xenon and nitrous oxide have been shown in 1998 to be effective inhibitors of the NMDA receptor (Franks et al., 1998; Jevtovic-Todorovic et al., 1998) which gave them potentially interesting neuroprotective properties for treating major brain insults such as cerebral ischemia. Cerebral ischemia is indeed a major health problem, constituting the third cause of mortality and the first cause of morbidity in industrialized countries. Cerebral stroke is provoked by an acute interruption of the cerebral blood flow, leading to an oxygen and glucose deprivation for the brain, inducing dramatic dysfunctions in the excitatory glutamatergic neurotransmission. The resulting toxic accumulation of glutamate leads to an over-stimulation of glutamatergic receptors like the NMDA receptors, this process is called glutamate excitotoxicity (Choi et al., 1988; Dirnagl et al., 1999; Lo et al., 2005). The use of NMDA receptor antagonists to block the neurotoxic cascade initiated by the glutamate has not yet been proven to be clinically efficient in humans, because of the intrinsic neurotoxicity of these chemical compounds (Olney et al., 1991). The only treatment today is the use of a thrombolytic agent, the tissue-type plasminogen activator (tPA), which degrades the insoluble fibrin clots (NINDS, 1995). However, this treatment is only applicable in a few number of cases, due to the hemorrhagic risk which shorten the therapeutic window (Lee et al., 1999; Ahmed et al., 2010). The research of new neuroprotective drugs thus constitutes a major therapeutic goal. Inert gases are a new class of therapeutic agents which have a remarkably safe clinical profile and readily cross the blood brain barrier. Moreover, they have low solubility in blood, which is advantageous in terms of rapid inflow and washout. Gases have thus the great advantages to present a reducing risk of neurotoxic side effects, compared to chemical neuroprotective drugs, especially at the low concentrations used for neuroprotection.

Nitrous oxide and xenon reduce ischemic neuronal death in an *in-vivo* model of transient cerebral ischemia in rats and decrease the NMDA-induced Ca^{2+} influx on neuronal cell cultures studied by *in-vitro* calcium video microscopy (David et al., 2003). These two gases produce the same effect than memantine, a low-affinity antagonist of NMDA receptor which is already used in clinics for neurodegenerative disease treatments (David et al., 2006). Investigations in rodents have confirmed that xenon at subanesthetic concentrations of about 50 vol% provides maximal neuroprotection, even when given 2 to 4 h after the insult onset (Ma et al., 2005; Dingley et al., 2006; David et al., 2008). Nitrous oxide (Haelewyn et al., 2008) and argon (David et al., submitted) which are less expensive gases than xenon, possess mild-to-moderate neuroprotective properties against excitotoxic insults and hypoxic-ischemic injuries.

However, xenon and nitrous oxide inhibit tPA-induced thrombolysis, preventing their use during the intra-ischemic period. When administrated after the reperfusion, xenon has beneficial effect by suppressing ischemic brain damage and tPA-induced brain hemorrhages

(David et al., 2010) while nitrous oxide reduces ischemic brain damage but increases tPA-induced brain hemorrages (Haelewyn et al., 2011).

Xenon is thus a very promising neuroprotective drug with few or no adverse side effects in models of acute ischemic stroke or perinatal hypoxia-ischemia (Homi et al., 2003; Ma et al., 2003; Abraini et al., 2005; David et al., 2008; Luo et al., 2008). Despite this, the widespread clinical use of xenon is limited by its scarceness and excessive cost of production, even if close xenon delivery systems are now being developed.

Using a mixture of xenon and another anesthetic gas like nitrous oxide (Marassio et al., 2011), argon (David et al., submitted), or helium (David et al., 2009) could combine the efficiency of xenon and the low cost and availability of the second gas and is thought to be a cost-efficient strategy.

Argon is an inert gas which is easily available and has no narcotic nor anesthetic action at ambient pressure. It presents some mild to moderate neuroprotective properties (David et al., submitted). Argon, contrary to xenon and nitrous oxide, may act directly by potentiating GABA neurotransmission at the $GABA_A$ receptor (Abraini et al., 2003).

Krypton is significantly less potent as an anesthetic agent than xenon, consistently with the Meyer-Overton rule which shows that krypton anesthetic potency is four fold less than xenon potency (Cullen et al., 1951; Kennedy et al., 1992).

Xenon, which has the highest solubility in lipids, also has the highest anesthetic potency (i.e. the lowest MAC-immobility) compared to krypton and argon (Table 1). Xenon also has the highest polarizability due to its high number of electron, compared to krypton and argon, so is predicted to be the gas which interact the most with proteins (Quillin et al., 2000).

Gas	Number of electrons	Polarizability ($Å^3$)	van der Waals radius (Å)	Solubility in lipids	MAC-immobility (bar)
Ar	18	1.64	1.91	0.14	27
Kr	36	2.48	2.03	0.43	7.31
Xe	54	4.04	2.21	1.17	1.61

Table 1. Physical and anesthetic properties of argon, krypton and xenon (from (Koblin et al., 1998; Quillin et al., 2000; Ruzicka et al., 2007)).

2. Determination of crystallographic structures of proteins under inert gases pressure

To investigate the mechanism of interaction of gases with proteins, a structural approach using protein crystallography under gas pressure was developed. Xenon binds reversibly to proteins through non-covalent, weak energy van der Waals forces (Ewing et al., 1970). The first structures of protein – xenon complexes were solved in 1965 with myoglobin and haemoglobin under a xenon pressure of 2.5 bar, evidencing a xenon binding site in these two globins (Schoenborn, 1965; Schoenborn et al., 1965). At a pressure of 7 bar, four xenon binding sites were found in myoglobin indicating that the number of xenon binding sites rises with pressure (Tilton et al., 1984).

Since then, many structures of protein-xenon complexes were solved, with xenon used as a heavy atom in isomorphous replacement phasing method (MIR), because xenon has a high

number of electrons (54 e^-) and binds with very little perturbation of the protein structure (Vitali et al., 1991; Schiltz et al., 1994; Bourguet et al., 1995; Colloc'h et al., 1997). On the other hand, krypton, though lighter than xenon, was popularized as an internal reference in anomalous phasing techniques MAD or SAD (Schiltz et al., 1997; Cohen et al., 2001) thanks to its absoption K edge at a convenient and useful wavelength easy to tune at all synchrotron places; for a review, see (Schiltz et al., 2003).

Xenon and other noble gas binds primarily in pre-existing hydrophobic cavities or pockets, very often empty in the native gas-less structures (Prangé et al., 1998). Xenon diffusing through protein atoms reaches easily its completely buried binding sites. Xenon was also used as an oxygen probe, based on the hypothesis that xenon and dioxygen would have equivalent binding sites (Duff et al., 2004). The comparison of the binding mode of xenon, krypton and argon was done on the phage T4 lysozyme, showing that gas occupancy rises with gas size and polarizability (Xe > Kr > Ar) (Quillin et al., 2000).

X-ray diffraction data of a protein under xenon pressure are collected either at liquid nitrogen temperature (100 K) or at room temperature. In the first case, the crystal inserted in a cryo-loop is placed in a xenon pressure chamber for a given time, then immediately after frozen in liquid nitrogen, to minimize the amount of xenon which could escape the protein crystal. The determination of the gas pressure within the crystal is thus quite imprecise. For the present study which needs the determination of protein structures under a large range of gas pressures, we have used a pressurisation cell in capillary, designed and developed for the preparation of isomorphous xenon derivatives (Schiltz et al., 1994; Schiltz et al., 2003).

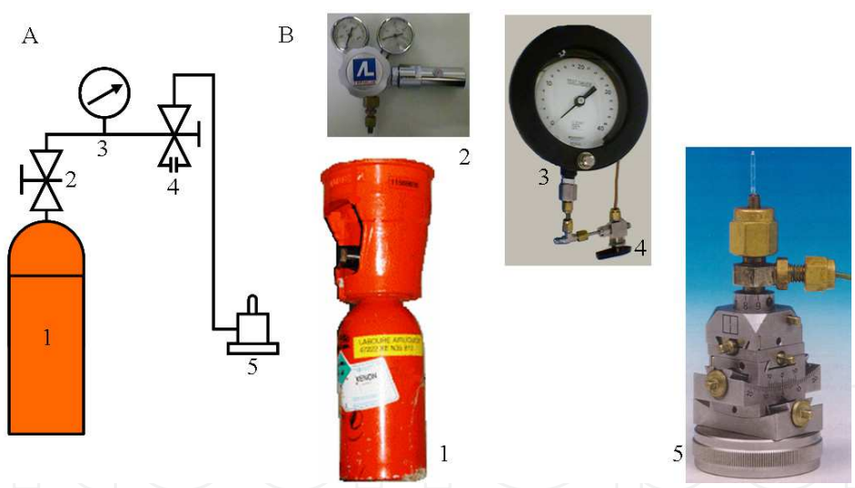

Fig. 1. The pressurisation cell setting. A. Connection between the five elements shown in B. 1- Xenon bottle, 2- Gas regulator, 3- High precision gauge, 4- Bleeding valve, 5- Pressurisation cell.

Typically, a crystal of protein is placed inside a quartz capillary mounted on the pressurisation cell. The pressurisation cell is fixed on a standard goniometer head, and connected to a gas bottle. The pressure within the cell is determined precisely with a calibrated Ashcroft precision gauge (Figure 1). The pressure is maintained constant during all the data collection.

For the present study, we have investigated three different enzymes, urate oxidase, elastase and lysozyme in complex with three gases, xenon, krypton and argon. In urate oxidase,

xenon binds primarily in a large buried hydrophobic cavity close to the active site (Colloc'h et al., 2007; Marassio et al., 2011). Xenon was used as an isomorphous derivative during the determination of urate oxidase structure (Colloc'h et al., 1997). In elastase, like in most of the serine proteases, xenon binds within the specificity pocket S1 of the active site (Schiltz et al., 1995). In lysozyme, xenon binds weakly in an internal cavity and mainly in a pocket located at a crystallographic interface (Schiltz et al., 1997; Prangé et al., 1998).

One of the drawbacks of using X-ray crystallography is the requirement to have a high gas pressure to be able to observe it in the electron density map. A gas pressure about 5 to 10 fold the physiological concentration is estimated to correspond to physiological conditions (Miller, 2002). In the present study, gas pressure ranges from 1 to 40 bar in order to reach a maximum occupancy at saturation, however, only the data between 5 and 10 bar can be compared to physiological conditions.

In the present study, diffraction data were collected at room temperature at the BM14, BM16 and BM30A beamlines at the European Synchrotron Radiation Facility (Grenoble, France). Detectors used were a MAR CCD detector for BM14, an ADSC Q210r CCD detector for BM16 and an ADSC Q315r CCD detector for BM30A. Data were indexed and integrated by *DENZO* and scaled independently and reduced using *SCALEPACK*, both programs from the *HKL* package (Otwinowski et al., 1997) or indexed and integrated by *MOSFLM* (Leslie, 2006) or *XDS* (Kabsch, 2010) and scaled by *SCALA*; intensities were converted in structure factor amplitudes and put on absolute scale using *TRUNCATE* and structure refinements were carried out by *REFMAC* (Murshudov et al., 1997), all programs from the *CCP4* package (Collaborative Computational Project, 1994). The graphics program *COOT* (Emsley et al., 2004) was used to visualize $|2Fobs - Fcalc|$ and $|Fobs - Fcalc|$ electron density maps and for manual rebuilding. Cavity volume were calculated with the program *CastP* (Dundas et al., 2006) with a probe radius of 1.3 Å. Structural figures were prepared using *PyMol* (deLano W.L., DeLano Scientific, Palo Alto, CA, USA).

3. Structure of urate oxidase under inert gas pressure

3.1 Structure of urate oxidase under pressure of xenon and nitrous oxide and comparison with *in-vivo* pharmacology effects

Aspergillus flavus urate oxidase (EC 1.7.3.3) is a homotetrameric enzyme of 301 residues per subunit which is involved in the oxidation of uric acid in presence of molecular oxygen. It crystallizes in the orthorhombic space group I222 with one monomer per asymmetric unit (cell: a = 79.8 Å, b = 96.2 Å, c = 105.4 Å, $\alpha = \beta = \gamma = 90°$). X-ray structures of urate oxidase under various pressures of xenon and nitrous oxide have been determined. Both gases were bound mainly in an internal cavity close to the active site of the enzyme, this cavity being empty in the native gas-less structure (Figure 2). This cavity, completely buried within the monomer, is highly hydrophobic, with 86 % of the atoms lining the cavity being carbons. Both gases were bound also very weakly to a second location, a small extension of a solvent-accessible pocket quite hydrophobic (lined by 75 % carbons). The gas occupancy in this second binding site remained very low (less than 30 % at 30 bar of pressure). Gas occupancies in the main binding site were high, reaching saturation at 100 % for xenon and 60 % for nitrous oxide (Table 2). The main effect of the gas was to expand the volume of the cavity where it binds. This expansion increased with gas occupancy and hence with gas pressure.

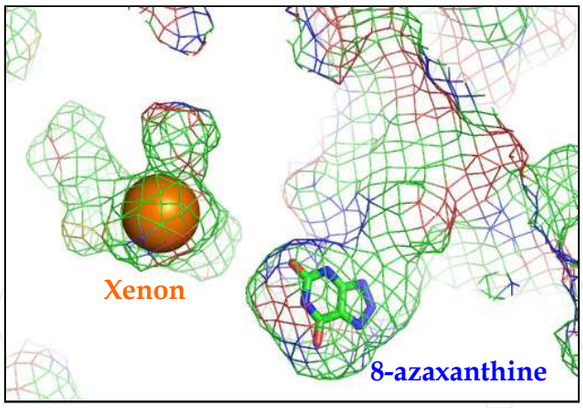

Fig. 2. Hydrophobic cavity in urate oxidase where xenon is bound (shown as an orange sphere). This cavity is close to the active site, where the competitive inhibitor 8-azaxanthine is located (colored in stick by atomic type). The solvent-accessible surface is shown in mesh representation colored by atomic type.

The ratio of gas-induced expansion of the hydrophobic cavity volume for xenon and nitrous oxide in urate oxidase, which could be considered as a model of globular proteins where inert gases bind and whose activity is disrupted by their presence, ranged between 1.1 and 1.5, depending on the applied pressure (Table 2). For the pressures estimated to correspond to physiological conditions (i.e. 5-10 bar), this ratio ranged between 1.3 and 1.5.

Xenon pressure (bar)	Xe occ. (%) Main	Xe-induced expansion	N_2O occ. (%) main	N_2O-induced expansion (%)	Ratio Xe/N_2O-induced expansion	Xe occ. (%) 2nd	N_2O occ. (%) 2nd
5	18	10.8	0	8.5	1.3	0	0
10	60	18.8	40	12.4	1.5	10	0
15	100	19.5	50	17.8	1.1	20	0
20	100	23.1	60	18.4	1.3	22	0
30	100	23.2	60	20.1	1.2	27	25

Table 2. Gas pressure, xenon and nitrous oxide occupancies in the main binding site, gas-induced expansion of the main gas binding site, ratio of expansion, and xenon and nitrous oxide occupancies in the secondary binding site.

If we compared these data with *in-vivo* pharmacology studies, we noticed that this ratio corresponded to the ratio of the narcotic potency of xenon compared to nitrous oxide (about 1.38) as estimated by the concentration of gas necessary to induce loss of righting reflex in rodents (Koblin et al., 1998; David et al., 2003), considered to be a behavioural endpoint closely related to MAC-awake (Campagna et al., 2003).

In comparison, the ratio of gas-induced volume expansion for xenon and nitrous oxide in annexin V, a protein which could be considered as a prototype of NMDA receptor for its properties of ion selectivity and voltage gating (Demange et al., 1994), did not correspond to the ratio of anesthetic potency of xenon and nitrous oxide. However, when considering urate oxidase and annexin V together as a model of simultaneous occupancy of globular proteins and ion-channel receptors, the ratio of gas-induced expansion for xenon and

nitrous oxide was close to 1, a value that corresponded to the ratio of anesthetic potency of xenon compared to nitrous oxide, as assessed by their MAC-immobility (Russell et al., 1992; Koblin et al., 1998).

These relationships between gas-induced structural effect and gas-induced narcotic effect allowed proposing a step-by-step mechanism of anesthesia. Gas would first bind to globular cytosolic or extracellular proteins which possess suitable gas binding site easily accessible. Gas-induced disruption of their function would lead to the early stages of anesthesia, i.e. amnesia and hypnosis. When all easily accessible gas binding sites are occupied, gas would then bind to neuronal channel which possess smaller gas binding sites, the disruption of their function would lead to surgical anesthesia, i.e. deep sedation and lack of responses to noxious stimuli (Colloc'h et al., 2007).

3.2 Structure of urate oxidase under pressure of xenon and nitrous oxide and comparison with *in-vitro* activity assays

As mentioned above, the main gas binding site in urate oxidase is very close to the active site (Figure 2). To investigate if gas occupancy and gas-induced volume expansion may have some functional relevance, we performed activity assays on urate oxidase in presence either of air, and either of a mixture of 75 vol % xenon or nitrous oxide and 25 vol % oxygen. To evaluate the alternative therapeutic strategy of using a mixture of xenon and nitrous oxide to combine the efficiency of xenon and the low cost and availability of nitrous oxide, we have also determined the structure of urate oxidase with various pressure of an equimolar mixture of xenon and nitrous oxide, and we have performed an activity assay in presence of a mixture of 37.5 vol% xenon, 37.5 vol% N_2O and 25 vol% oxygen. We found that Xe:N_2O induced a higher expansion of the cavity volume than pure xenon, which in turn induced a higher expansion than N_2O as seen above. *In-vitro* activity assays revealed that Xe:N_2O-induced inhibition was higher than Xe-induced inhibition, itself higher than N_2O-induced inhibition. The relationship between structural effect of the gas, i.e. gas-induced volume expansion, and the functional effect of the gas, i.e. gas-induced inhibition of the enzymatic reaction, highlighted the way by which gases might disrupt protein function through an indirect mechanism (Marassio et al., 2011).

The role of the void hydrophobic cavity in the catalytic mechanism was thus demonstrated by the activity assays in presence of gas. This functional role was also suggested by the high-pressure structural and functional study of urate oxidase. Under high hydrostatic pressure (150 Ma; 1500 bar) the volume of the cavity was reduced as expected, while the volume of the active site was expanded. High pressure also inhibited the catalytic mechanism of urate oxidase, this loss of activity being a loss of substrate affinity (Girard et al., 2010).

In both cases (gas or pressure), there was a loss of flexibility of the cavity, either by the gas presence which induced an expansion and inhibited its contraction, either by high pressure which induced a cavity contraction but inhibited its expansion. The role of the cavity in the functional mechanism of urate oxidase seems then to give some flexibility to the active site to allow a structural fit for the ligand in the active site.

3.3 Structure of urate oxidase under pressure of krypton and comparison with gas solubility in lipids

Structures of urate oxidase under krypton pressure of 2 to 30 bar were determined in the present study. Krypton was bound to the exact same location than xenon, in the

hydrophobic cavity close to the active site. Krypton occupancy increased with the applied pressure up to 45 % at 30 bar (Table 3). Like xenon, krypton was also weakly bound to a secondary binding site at the bottom of a solvent-accessible pocket, but only at pressure above 20 bar.

For an identical pressure, krypton occupancy was always lower than xenon occupancy (Figure 3A). Xenon which has a higher number of electrons than krypton has a higher polarizability (Table 1) and binds thus with a higher occupancy, as already observed in the case of phage T4 lysozyme (Quillin et al., 2000).

Krypton pressure (bar)	Resolution (Å)	Occ. in main binding site (%)	Kr-induced expansion (%)	Xe-induced expansion (%)	Ratio Xe / Kr induced expansion	Occ. in 2nd binding site (%)
2	1.60	10	3.2	3.3	1.0	0
5	1.60	15	4.1	10.8	2.6	0
10	1.55	20	11.4	18.8	1.6	0
20	1.65	40	12.8	23.1	1.8	10
30	1.65	45	15.2	23.2	1.5	15

Table 3. Krypton pressure, resolution of the crystallographic structure, krypton occupancy in the main binding site, krypton-induced and xenon-induced volume expansion of the main binding site, ratio of the Xe and Kr-induced volume expansion and krypton occupancy in the secondary binding site.

If one refers to the Meyer-Overton rule, the narcotic potency of a gas would be related to its solubility in lipids. The ratio of solubility in lipids of xenon compared to krypton is 1.17 / 0.14 = 2.7 (Table 1), a value which correspond to the ratio of Xe and Kr-induced volume expansion at the pressure of 5 bar, well within the range of pressure estimated to correspond to physiological condition. This result confirmed what was shown previously when comparing the structural-induced effect of xenon and nitrous oxide on urate oxidase to their in-vivo effect as evaluated by their MAC-awake (Colloc'h et al., 2007). However, the MAC-immobility which prevents response to noxious stimuli for xenon in man is about 4.5 higher than the MAC-immobility of krypton (Table 1), which does not correspond to the structural Xe- and Kr-induced structural effect in urate oxidase, considered as a model for globular protein whose function is disrupted by the presence of gas.

3.4 Structure of urate oxidase under pressure of argon and comparison with *in-vivo* pharmacology study

Structures of urate oxidase under argon pressure of 10 to 65 bar were determined in the present study. Argon was bound to the exact same location than xenon and krypton, in the large hydrophobic cavity close to the active site. Argon became visible in the electron density map at a pressure of 30 bar and above, with an occupancy factor of 40 % at a pressure of 65 bar (Table 4). 65 bar is the maximum pressure which could be reach in the quartz capillary; above that pressure, the risk of breakage of the capillary became very high. At the same pressure, argon occupancy was always lower than krypton and xenon occupancies (Figure 3A). In the secondary binding site where xenon and krypton bind very weakly, no argon is detectable in the electron density map, even at a pressure of 65 bar.

Argon pressure (bar)	Resolution (Å)	Occ. in main binding site (%)	Ar-induced expansion (%)	Xe-induced expansion (%)	Ratio Xe / Ar Indiced expansion
10	1.65	0	7.1	20.7	2.9
20	1.90	0	11.0	24.6	2.2
25	1.60	20	13.4		
30	1.60	20	12.3	24.6	2
35	1.60	20	14.1		
40	1.75	20	10.3		
45	1.60	25	11.1		
55	1.60	30	10.7		
65	1.60	40	16.4		

Table 4. Argon pressure, resolution of the crystallographic structure, argon occupancy, argon-induced and xenon-induced cavity volume expansion, and ratio of the Xe and Ar-induced volume expansion.

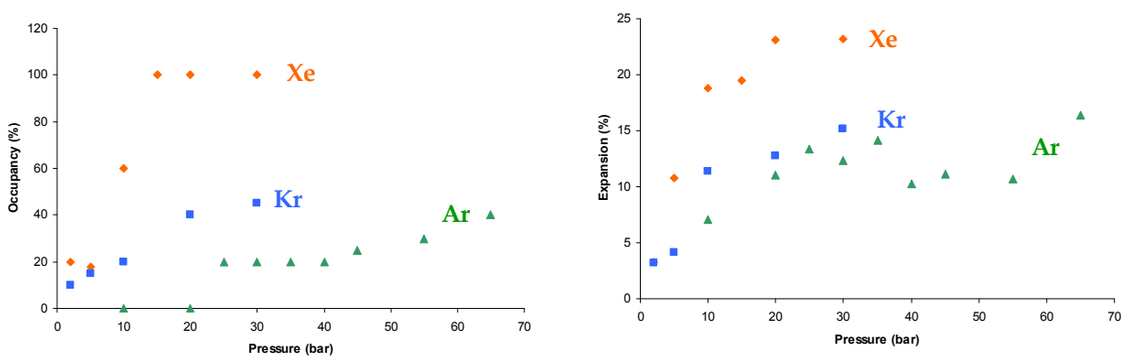

Fig. 3. A. Gas occupancy as a function of pressure. B. Gas-induced expansion of the main binding site as a function of pressure.

As for the two other nobles gas, the main effect of argon was to expand the volume of the cavity where it was bound. However, due to its quite low occupancy factor and its small size, the argon-induced expansion remained low, around 10 % of expansion except for the pressure of 65 bar where expansion reached 16 % (Table 4). For pressure of 10 and 20 bar where argon was not detectable in the electron density map, there was already a volume expansion indicating with little doubt the presence of argon within the cavity (Table 4, Figure 3B).

The ratio of Xe- and Ar-induced expansions of the cavity volume was 2.9 for a pressure of 10 bar, which did not correspond to their inverse ratio of MAC-immobility (27/1.61 = 16.8) nor their ratio of solubility in lipids (1.17 / 0.14 = 8.4) (Table 1). However, argon is not narcotic at ambient pressure and needs to be pressurised to have some narcotic action.

In order to allow comparison of the effects of argon and xenon in urate oxidase, we further calculated the theoretical expansion of the gas binding cavity produced by argon at 100 % occupancy according to a linear regression model. For occupancy of 100% of argon, the corresponding volume expansion would be of 23.3 % (Figure 4A). According to a linear

regression model, this expansion would be reach for a pressure of 164 bar (Figure 4B). This pressure corresponds to about ten fold the pressure of 14 to 17 bar at which argon is known to produces narcosis in rodents (Abraini et al., 1998; Koblin et al., 1998).

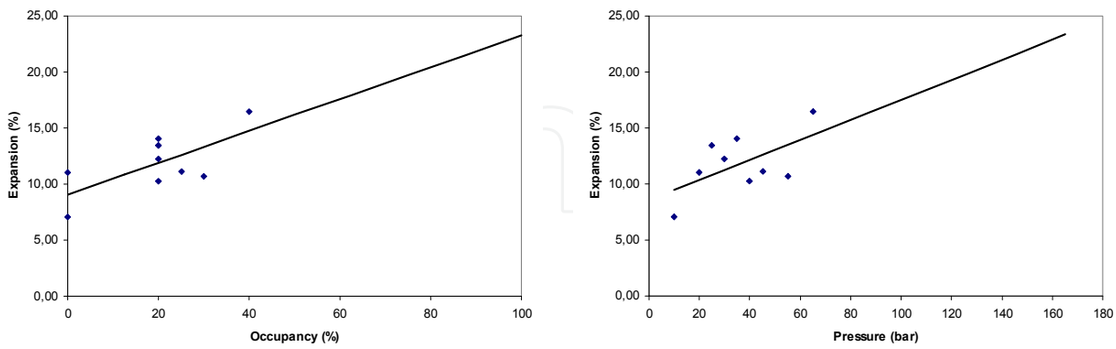

Fig. 4. Linear regression model for cavity volume expansion as a function of occupancy (A) and as a function of pressure (B).

In addition, it should be mentioned that these estimated values for argon were also consistent with crystallographic data that have demonstrated that xenon at full occupancy (pressure of about 20 bar) produces a similar maximal expansion around 23-25 % of the gas binding site (Table 2). This is consistent with the fact that the ratio between the efficient estimated pressure of argon and the efficient experimental pressure of xenon at producing full occupancy and maximal expansion of the gas binding site (164 / 20 = 8.2) is similar to the ratio of their solubility in lipids (1.17 / 0.14 = 8.4) as predicted by the Meyer-Overton rule (Abraini et al., 2003; Campagna et al., 2003).

Argon is narcotic only in hyperbaric condition. At ambient pressure, argon may thus have a very limited influence on its target function. Since one of the major effect of hydrostatic pressure is to contract the volume of internal cavities (Girard et al., 2010), it may explain why argon needs hyperbaric condition to exert its influence.

3.5 Conclusion on urate oxidase structures under inert gas pressure

The three noble gases were bound to an identical location in urate oxidase, within an internal hydrophobic cavity. The gas occupancies increased in the sequence argon < krypton < xenon, as it was the case for T4 lysozyme (Quillin et al., 2000), who noticed that smaller gases do not bind as well as larger ones as a result of their attenuated polarizability. Xenon and krypton were bound also weakly in a secondary binding site, while argon was not observed even at high pressure.

The main effect of the gas was to expand the cavity volume where it binds. The ratio of expansion was related to the narcotic potency of the gas, as evaluated by their MAC-awake or their solubility in lipids. The presence of xenon within the cavity induced an inhibition of the catalytic mechanism, with a relationship between gas-induced expansion and gas-induced inhibition, as shown by the comparison between xenon and nitrous oxide structural and functional effects. No activity assays were performed in presence of krypton or argon, but we can predict, based on the present structural results, that krypton should induce an inhibition of the catalytic mechanism of urate oxidase. However, krypton-induced inhibition should be lower than xenon-induced inhibition, according to their relative induced

expansion in the range 5-10 bar (Table 3). Argon-induced inhibition should be very low or inexistent, according to the very low gas occupancy and argon-induced expansion at a pressure of 10 bar (Table 4).

4. Structure of elastase under inert gas pressure

4.1 Introduction on elastase structures under inert gas pressure

Pancreatic porcine elastase (EC 3.4.21.36) is a serine protease of 266 residues which hydrolyzes peptide bonds in proteins, its main substrate being elastine. The catalytic triad of elastase is composed, as for all serine proteases, of an activated serine (Ser 195) assisted by a proton relay (His 57), which acts as a general base, and stabilized through an hydrogen bond by an aspartic acid (Asp 102). Pancreatic porcine elastase crystallizes in the orthorhombic space group $P2_12_12_1$ with one monomeric enzyme per asymmetric unit (cell : a = 51.4 Å, b = 58.0 Å, c = 75.3 Å, $\alpha = \beta = \gamma = 90°$). In the crystallographic structure, a sulphate or an acetate ion is bound in the oxyanion hole, depending on the concentration of the precipitating agents. The primary specificity pocket S1 is a hydrophobic pocket located below the oxyanion hole and the Ser 195 which is specific for recognition of the peptidic substrate.

In the crystallographic structures of apo elastase, the S1 pocket was either empty, either filled by a water molecule hydrogen-bonded to a water molecule outside of the S1 pocket and to an oxygen atom of the sulphate ion (Figure 5A). When this water molecule (termed W-S1) was present, its B-factor was quite elevated. In the different crystallographic structures of elestase in complex with xenon deposited in the Protein Data Bank, 1C1M (Schiltz et al., 1995), 1L1G and 1L0Z (Panjikar et al., 2002), 1UO6 and 2A7C (Mueller-Dieckmann et al., 2004) and 2OQU (Kim et al., 2007), xenon was bound within the specificity pocket S1 in the active site of elastase (Figure 5B). This xenon binding site is moderately hydrophobic, lined with 60% carbons.

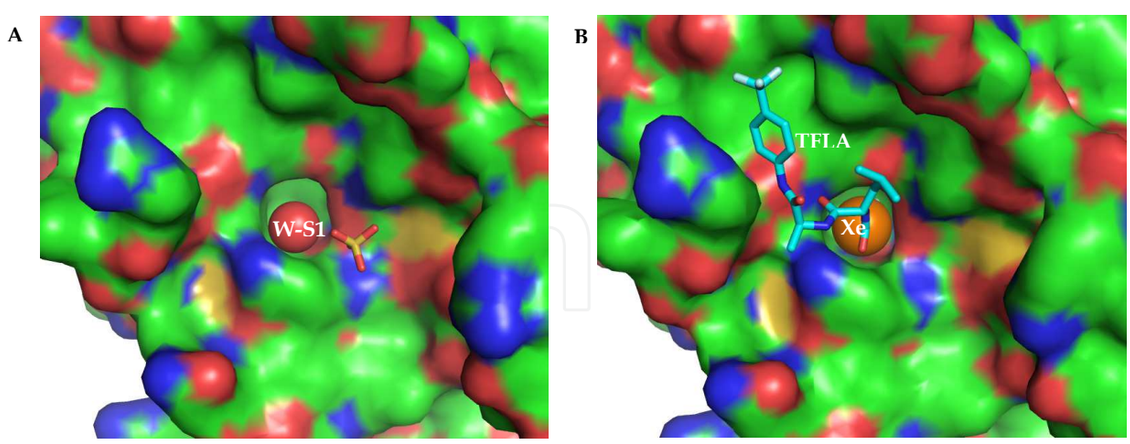

Fig. 5. Elastase shown with its solvent-accessible surface colored by atomic type. A. Native gas-less elastase with the water molecule W-S1 in the S1 pocket. B. Elastase in complex with xenon (shown as an orange sphere) or in complex with a peptidic inhibitor TFLA (shown in cyan in stick representation).

In the present study, structures of native elastase (gas-less) were determined in the same conditions than structures under inert gas pressure, i.e. at room temperature in a quartz

capillary. Three structures have been solved, at 1.38 Å, 1.7 Å and 1.45 Å resolution. In two native structures, the S1 pocket was empty while in one of them, there was the water molecule W-S1 with a B-factor of 36.3 Å^2.

4.2 Structure of elastase under pressure of xenon and comparison with *in-vitro* activity assays

Structures of elastase under xenon pressure from 1 bar to 30 bar were determined in the present study. Whatever the applied pressure, xenon was bound to a unique site, within the specificity pocket S1, with an occupancy which increased with the applied pressure. Occupancy reached 100 % for a pressure of 30 bar (Table 5). The S1 pocket where xenon binds is moderately hydrophobic, with 60 % of atoms lining it being carbons. This gas binding site is less hydrophobic than the main gas binding site in urate oxidase, which was lined by 86 % carbons. The atom the closest to xenon is the side chain atom Oγ of the catalytic Ser 195.

Xenon pressure (bar)	Resolution (Å)	Occ. (%)	Xe-induced expansion (%)
1	1.40	15	3.0
2	1.45	25	3.3
5	1.50	30	7.8
10	1.50	70	9.4
20	1.60	90	12.7
30	1.65	100	13.6

Table 5. Xenon pressure, resolution of the crystallographic structure, occupancy and xenon-induced expansion of the S1 pocket in elastase.

Whatever the pressure, there was no water molecules in the S1 pocket, so if the water molecule W-S1 was present in the native gas-less structure, it was not displaced but replaced by xenon. However, xenon did not take the exact location of the W-S1 and was closer to the Oγ of the catalytic Ser 195 (3.4 Å instead of 3.8 Å).

The presence of xenon within the S1 pocket expanded its volume, its expansion rising with the applied pressure. However, since the gas was bound directly within the active site, the gas-induced inhibition is likely to be a direct inhibition and the expansion by itself has probably no functional relevance. Xenon took indeed the place of peptidic inhibitors, like the trifluroacetyl-leu-ala (TFLA) known to be an excellent inhibitor of elastase (Li de la Sierra et al., 1990) (Figure 5B).

To investigate the direct inhibition by xenon, we performed activity assays on elastase in presence either of air, either of 100 vol % xenon. Initial velocity in presence of xenon when compared to air (taken as 100 %) was 81.5 + 2.1 % revealing an inhibition of the catalytic activity of elastase of around 20 % by xenon. However, this inhibition was lower than xenon occupation in the range 5-10 bar (30 – 70 % occupation).

Tissue-type plasminogen activator (tPA), the only approved treatment for thrombolysis after an ischemic stroke, is also a serine protease. As in the case of elastase, xenon inhibited tPA enzymatic activity (David et al., 2010). This inhibition is likely to be a direct inhibition with xenon binding directly in the S1 pocket in the active site of tPA. Serine proteases have

indeed structurally similar active site with the same catalytic triad which can be easily superimposed (Schiltz et al., 1995). The superimposition of the catalytic triad of elastase and of tPA suggested that xenon fitted perfectly in the S1 pocket of tPA, thus inhibiting tPA enzymatic activity.

4.3 Structure of elastase under pressure of krypton

Structures of elastase under pressure of krypton from 2 to 30 bar were determined in the present study. Krypton was bound within the S1 pocket, at the exact same location than xenon. The water molecule W-S1 if it was present was replaced by the krypton atom. Occupancy of krypton reached 70 % at the pressure of 30 bar (Table 6).

Krypton pressure (bar)	Resolution (Å)	Occ. (%)	Kr-induced expansion (%)
2	1.35	20	4.9
5	1.45	25	4.9
10	1.50	35	5.8
20	1.75	50	7.9
30	1.45	70	8.5

Table 6. Krypton pressure, resolution of the crystallographic structure, occupancy and krypton-induced expansion of the S1 pocket in elastase.

Krypton occupancy was always lower than xenon occupancy for a same pressure (Figure 6). Xenon which is more polarizable was bound with a higher occupancy than krypton. Since the gas binding site is only moderately hydrophobic, with a lot of polar atoms lining the gas, it is likely that dipole-induced interactions play an important role in gas binding. Like xenon, krypton induced an expansion of the S1 pocket where it binds. However, this expansion remained quite low, less than 10 %.

4.4 Structure of elastase under pressure of argon

Structures of elastase under pressure of argon of 10 to 60 bar were determined in the present study. Argon was bound within the S1 pocket, at the exact same location than xenon and krypton. Argon occupancy reached 50 % for a pressure of 60 bar (Table 7). For technical conditions, it was not possible to reach higher pressure due to the risk of failure of the quartz capillary. Argon occupancy was always lower than krypton and xenon occupancy for a same pressure, according to a lower polarizablity (Figure 6).

Argon pressure (bar)	Resolution (Å)	Occ. (%)	B factor W-S1
10	1.35	35	42.5
20	1.45	35	missing
30	1.50	40	40.1
40	1.35	40	missing
60	1.50	50	missing

Table 7. Argon pressure, resolution of the crystallographic structure, occupancy and B-factor of the water molecule W-S1 if it is present.

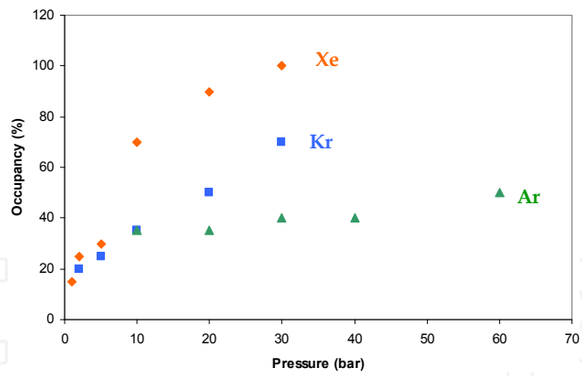

Fig. 6. Xenon, krypton and argon occupancies as a function of pressure.

Argon occupancy was higher in elastase than in urate oxidase (Table 4), probably because of the smaller size of the gas binding site in elastase which would allow a better binding of argon.

Argon-induced expansion of the S1 pocket was very low and not very significant (less than 5 %), probably due to the small size of the argon atom.

Contrary to xenon and krypton cases, when the water molecule W-S1 was present in the native gas-less structure, this water molecule remained visible close to the argon electronic density (Figure 7), with a lower occupation factor. The distance between the argon atom and the W-S1 molecule was about 2.8 Å.

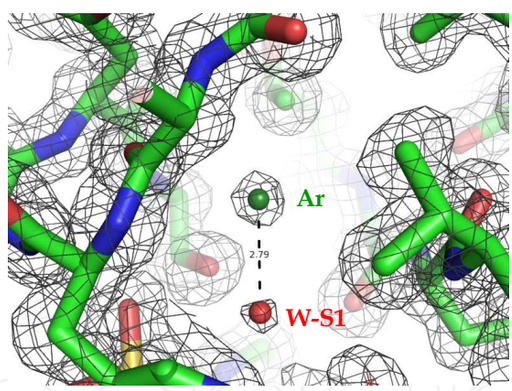

Fig. 7. *2Fo-Fc* electron density map of elastase under an argon pressure of 10 bar, contoured at 1 σ.

4.5 Conclusion on elastase structures under inert gas pressure

In elastase, there is one unique gas binding site, located within the S1 pocket in the active site. Contrary to urate oxidase where the gas binding site was an empty cavity, there might be a water molecule in the moderately hydrophobic S1 pocket. When present, this water molecule was replaced by xenon and krypton, but remained visible close to argon.

Xenon inhibited directly elastase catalytic activity by taking the place of the substrate, even if its inhibition stayed lower than its occupancy. It is also likely that krypton inhibited elastase catalytic activity. Since krypton occupancy was lower than xenon occupancy, krypton-induced inhibition is expected to be lower than xenon-induced inhibition. In the range 5-10 bar, krypton occupancy ranged between 25 and 35%, inducing probably a rather

small inhibition of the enzymatic reaction. Argon-induced inhibition of the catalytic reaction is likely to be quite low and similar to krypton-induced inhibition, with an occupation of argon of 35 % at 10 bar.

5. Structure of lysozyme under inert gas pressure

5.1 Introduction on lysozyme structures under inert gas pressure

Egg white lysozyme C (EC 3.2.1.17) is an enzyme of 129 residues which hydrolyse peptidoglycans. It crystallizes in tetragonal space group $P4_32_12$ with one monomeric enzyme per asymmetric unit (cell: a = 79.2 Å, b = 79.2 Å, c = 37.9 Å, $\alpha = \beta = \gamma = 90°$). In the different crystallographic structures of lysozyme in presence of xenon deposited in the Protein Data Bank : 1C10 (Prangé et al., 1998), 2A7D (Mueller-Dieckmann et al., 2004) and 1VAU (Takeda et al., 2004), xenon was bound mainly in a pocket at a crystallographic interface (gas binding site I or GBS I in Figure 8) and weakly in a small internal cavity (GBS II in Figure 8). In the native gas-less structure, a water molecule was present in GBS I, and GBS II was empty. GBS I is moderately hydrophobic, lined with 55 % carbons, and GBS II is very hydrophobic, lined with 83 % carbons. The occupancy of xenon ranged between 30 and 60% in GBS I and stayed beyond 25 % in GBS II.

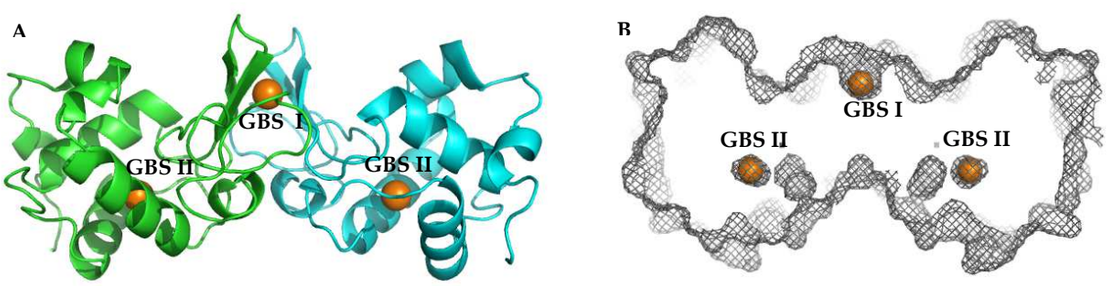

Fig. 8. Xenon binding sites in lysozyme, shown with two symmetrical subunits. A. Xenon was bound at the crystallographic interface between two symmetrical monomers (GBS I) and a second xenon was bound within a small internal cavity buried within each monomer (GBS II) (xenon shown as orange spheres, and lysozyme with its Cα chain as ribbon, one symmetric is colored in green, the second in blue). B. Solvent-accessible surface of two symmetrical lysozymes.

In the structure 1C10, a third xenon was located in the active site, where either two water molecules or one water molecule and one chloride ion were found in the other deposited structures. In the structure 1VAU, a third xenon was located in another crystallographic pocket at the interface between two monomers, where a water molecule was found in the other deposited structures.

In the crystallographic structure of lysozyme under a 55 bar pressure of krypton 1QTK, (Schiltz et al., 1997; Prangé et al., 1998), krypton was bound in the internal cavity (GBS II) but not in the crystallographic pocket (GBS I).

In the present study, the structure of a native gas-less lysozyme was determined in the same condition than structures under inert gas pressure, i.e. at room temperature in quartz capillary. Two native structures have been solved, at 1.6 Å and 1.55 Å resolution. In both structures, the internal cavity GBS II was empty and there was a water molecule in GBS I which had a B-

factor between 25 and 29 Å^2. The volume of the internal cavity GBS II is very small, about 40 Å^3 while the volume of GBS I at a crystallographic interface is larger, around 100 Å^3.

5.2 Structure of lysozyme under pressure of xenon

The structures of lysozyme under xenon pressure of 10 to 30 bar were determined in the present study. Xenon was bound in GBS I with an occupancy which did not increase with pressure and remained around 20 and 30 % (which is the double of the occupancy for the monomer since the xenon is located at a crystallographic interface). Xenon was also bound in GBS II with an occupancy which increased with the applied pressure but which remained quite low (20 % occupancy at 30 bar).

Xenon occupancy in GBS I remained stable whatever the applied pressure and induced almost no expansion of its volume (less than 10 %). Xenon location was not exactly superposed to the water molecule location present in the native gas-less structure, with a distance of 0.6 to 0.7 Å between them. This gas binding site being located at a crystallographic interface is likely to be not physiological.

Xenon pressure (bar)	Resolution (Å)	Xe occ. in GBS I (%)	Xe occ. in GBS II (%)	Xe-induced expansion of GBS II (%)
10	1.55	30	10	9.1
15	1.60	20	10	4.6
20	1.55	30	12	6.9
25	1.90	24	15	13.6
30	1.65	30	20	23.4

Table 8. Xenon pressure, resolution of the crystallographic structures, xenon occupancy in GBS I , xenon occupancy in GBS II and xenon-induced expansion of GBS II.

Xenon occupancy in GBS II remained very low, due to the small size of the cavity (volume around 40 Å^3). Xenon van der Waals radius is of 2.21 Å, its theoretical volume is thus of 45 Å^3, close to the volume of GBS II. Xenon induced an expansion of the volume of this small internal cavity which reached a volume around 50 Å^3 for xenon occupancy of 20 %. In the range of pressure corresponding to physiological conditions (5 – 10 bar), the occupation of xenon in GBS II is likely to be very small (less than 10 %).

5.3 Structure of lysozyme under pressure of krypton

The structures of lysozyme under krypton pressure of 5 to 20 bar were determined in the present study. No krypton was visible in GBS I whatever the applied pressure, as it was the case in the structure determined under a krypton pressure of 55 bar. In all cases, there was a water molecule at the exact same location than in the native gas-less structure. Krypton was bound weakly in GBS-II and became visible in the electron density map at a pressure of 20 bar. Krypton induced an expansion of the volume of GBS II which seemed not related to krypton occupancy. However, this krypton-induced expansion of GBS II indicated that krypton was present event when it was not visible in the electron density map (Table 9).

Krypton is smaller than xenon (van der Waals radius of 2.03 Å instead of 2.21 Å, and volume of 35 Å^3 instead of 45 Å^3), it is thus likely than krypton occupancy can reach higher value than xenon occupancy in GBS II (Figure 9).

Krypton pressure (bar)	Resolution (Å)	Kr occ. in GBS I (%)	Kr occ. in GBS II (%)	Kr-induced expansion of GBS II (%)
5	1.55	0	0	12.1
10	1.60	0	0	4.6
20	1.55	0	10	14.9
55 (1QTK)	2.03	0	49	7.1

Table 9. Krypton pressure, resolution of the crystallographic structures, krypton occupancy in GBS I , krypton occupancy in GBS II and krypton-induced expansion of GBS II.

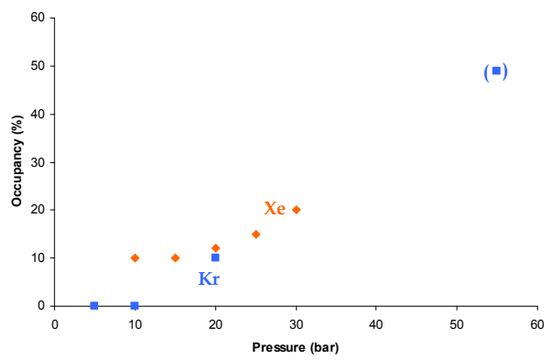

Fig. 9. Xenon and krypton occupancies as a function of pressure.

A theoretical study based on a three-dimensional distribution function theory of molecular liquids was applied to lysozyme in presence of water and noble gases (Imai et al., 2007). This study predicted that krypton had a slightly better affinity for GBS II than xenon. Structures of lysozyme under higher pressure of krypton (30 and 40 bar) would be necessary to confirm this prediction.

5.4 Structure of lysozyme under pressure of argon

The structures of lysozyme under argon pressure of 10 to 50 bar were determined in the present study. Whatever the applied pressure, no argon was visible in the electron density map even at a pressure of 50 bar neither in GBS I or in GBS II. In GBS I, the water molecule was present at the exact place of the water molecule in the native gas-less structure. The smaller size of argon should not prevent argon to bind within GBS II, however, a higher pressure would probably be necessary to be able to visualize argon in the electron density map in GBS II.

In the theoretical study already mentioned (Imai et al., 2007), argon affinity for GBS II was predicted to be very high. However, the present study showed that even at high pressure, argon did not bind within GBS II, even if it smaller size would allow its binding. Argon polarizability is lower than krypton and xenon polarizabilities (Table 1), due to its small number of electron, and could explain its very low affinity for lysozyme.

5.5 Conclusion on lysozyme structures under inert gas pressure

Lysozyme possesses two gas binding sites, one located in a pocket at a crystallographic interface (GBS I) and one located within a quite small internal cavity (GBS II). Both xenon

and krypton were bound within GBS II with a quite low occupation, and only xenon was bound within GBS I. Argon did not bind to lysozyme even at a pressure of 50 bar. The rule that showed that gas occupancy rose with gas size and polarizability is almost respected, since the small size of GBS II could prevent xenon binding and thus favour krypton binding.
In the pressure range which would correspond to physiological conditions (5 – 10 bar), xenon occupancy is likely to be very low (less than 10 %), and krypton and argon occupancies are null. It is then likely than enzymatic activity of lysozyme is not modified by the presence of an inert gas.

6. Conclusion

Noble gases bind to proteins essentially through non-covalent van der Waals interactions, their binding constant depending on their electronic polarizability. In the three studied enzymes, gas occupancies were in the order of their polarizability, Xe > Kr > Ar, as it was already found for T4 lysozyme (Quillin et al., 2000). The only slight exception was the internal cavity of egg white lysozyme, where its smaller size prevented xenon higher occupancy.
The major physiological targets of gaseous anesthetics are postulated to be neuronal channels receptors, like the NMDA receptor which is inhibited by xenon (Campagna et al., 2003; Franks, 2008), or the $GABA_A$ receptor which could be modulated by argon (Abraini et al., 2003). However, at lower concentration, gas would bind mainly to globular targets, amongst them enzymes, whose functions would be modulated by the presence of inert gas.
From the present study, we can infer different mode of inhibition by gas. In urate oxidase, gas inhibited the catalytic reaction through an indirect mechanism; the presence of the gas within the cavity would prevent the cavity contraction, thus modifying the active site flexibility. In elastase, gas inhibited the catalytic reaction through a direct mechanism; the presence of the gas in the active site would prevent the substrate binding. In lysozyme, gas would not inhibit the catalytic reaction, their occupation being too weak.
Protein activity requires some conformational flexibility (Frauenfelder et al., 1991). In enzymes, the balance between conformational flexibility and rigidity is adjusted to optimize the catalytic efficiency for a given condition (Chiuri et al., 2009). Cavities would facilitate conformational changes and are though to play a key role in protein function (Hubbard et al., 1994). Anesthetics have been postulated to act by stabilizing high-energy conformers inducing altered functions (Eckenhoff, 2001; Johansson et al., 2005). High pressure was also postulated to stabilize high-energy conformers with altered functions (Frauenfelder et al., 1990; Akasaka, 2006; Fourme et al., 2006). Urate oxidase is thus a key example which highlights the effect of anesthetic, since this enzyme is both inhibited by gas presence in a hydrophobic cavity (Marassio et al., 2011) and by high pressure (Girard et al., 2010).
Inert gas binds to proteins through very weak non-covalent van der waals interaction. How such weak interactions could generate such high biological effect such as anesthesia ? It was suggested that anesthesia would arise from small effects at many biological targets (Eckenhoff, 2001). The present study would confirm this hypothesis, showing that some enzymes could be stabilized by the presence of gas in hydrophobic cavity (as in urate oxidase), some enzymes could be directly inhibited by gas (as in elastase case), and some enzymes are not affected by gas (as in the case of lysozyme). The mechanisms of neuroprotection and anesthesia by inert gases are thus very complex processes with many biological targets whose function are modulated (inhibited or potentiated) by the presence of gas.

7. Acknowledgement

The authors thank Jacques H. Abraini (CI-NAPS, UMR 6232, Caen) for advises during this work.

8. References

Abraini, J.H., David, H.N. & Lemaire, M. (2005). Potentially neuroprotective and therapeutic properties of nitrous oxide and xenon. *Ann. N. Y. Acad. Sci.* Vol. 1053: pp. 289-300.

Abraini, J.H., Kriem, B., Balon, N., Rostain, J.C. & Risso, J.J. (2003). Gamma-aminobutyric acid neuropharmacological investigations on narcosis produced by nitrogen, argon, or nitrous oxide. *Anesth. Analg.* Vol. 96 No. 3: pp. 746-749.

Abraini, J.H., Rostain, J.C. & Kriem, B. (1998). Sigmoidal compression rate-dependence of inert gas narcotic potency in rats: implication for lipid vs. protein theories of inert gas action in the central nervous system. *Brain Res.* Vol. 808 No. 2: pp. 300-304.

Ahmed, N., Wahlgren, N., Grond, M., Hennerici, M., Lees, K.R., Mikulik, R., Parsons, M., Roine, R.O., Toni, D. & Ringleb, P. (2010). Implementation and outcome of thrombolysis with alteplase 3-4.5 h after an acute stroke: an updated analysis from SITS-ISTR. *Lancet Neurol.* Vol. 9 No. 9: pp. 866-874.

Akasaka, K. (2006). Probing conformational fluctuation of proteins by pressure perturbation. *Chem. Rev.* Vol. 106 No. 5: pp. 1814-1835.

Bourguet, W., Ruff, M., Chambon, P., Gronemeyer, H. & Moras, D. (1995). Crystal structure of the ligand-binding domain of the human nuclear receptor RXR-alpha. *Nature* Vol. 375 No. 6530: pp. 377-382.

Campagna, J.A., Miller, K.W. & Forman, S.A. (2003). Mechanisms of actions of inhaled anesthetics. *New Engl. J. Med.* Vol. 348 No. 21: pp. 2110-2124.

Chiuri, R., Maiorano, G., Rizzello, A., del Mercato, L.L., Cingolani, R., Rinaldi, R., Maffia, M. & Pompa, P.P. (2009). Exploring local flexibility/rigidity in psychrophilic and mesophilic carbonic anhydrases. *Biophys. J.* Vol. 96 No. 4: pp. 1586-1596.

Choi, D.W., Koh, J.Y. & Peters, S. (1988). Pharmacology of glutamate neurotoxicity in cortical cell culture: attenuation by NMDA antagonists. *J. Neurosci.* Vol. 8 No. 1: pp. 185-196.

Cohen, A., Ellis, P., Kresge, N. & Soltis, S.M. (2001). MAD phasing with krypton. *Acta Crystallogr.* Vol. D57 No. 2: pp. 233-238.

Collaborative Computational Project, Number 4. (1994). The *CCP4* suite : programs for protein crystallography. *Acta Crystallogr.* Vol. D50 No. 2: pp. 760-763.

Colloc'h, N., El Hajji, M., Bachet, B., L'Hermite, G., Schiltz, M., Prangé, T., Castro, B. & Mornon, J.P. (1997). Crystal structure of the protein drug urate oxidase-inhibitor complex at 2.05 Å resolution. *Nat. Struc. Biol.* Vol. 4 No. 11: pp. 947-952.

Colloc'h, N., Sopkova-de Oliveira Santos, J., Retailleau, P., Vivarès, D., Bonneté, F., Langlois d'Estaintot, B., Gallois, B., Brisson, A., Risso, J.J., Lemaire, M., Prangé, T. & Abraini, J.H. (2007). Protein crystallography under xenon and nitrous oxide pressure: comparison with in vivo pharmacology studies and implications for the mechanism of inhaled anesthetic action. *Biophys. J.* Vol. 92 No. 1: pp. 217-224.

Cullen, S.C. & Gross, E.G. (1951). The anesthetic properties of xenon in human and animal beings, with additional observations on krypton. *Science* Vol. 113 No. 2942: pp. 580-582.

David, H.N., Ansseau, M., Lemaire, M. & Abraini, J.H. (2006). Nitrous oxide and xenon prevent amphetamine-induced carrier-mediated dopamine release in a memantine-like fashion and protect against behavioral sensitization. *Biol. Psychiatry* Vol. 60 No. 1: pp. 49-57.

David, H.N., Haelewyn, B., Chazalviel, L., Lecocq, M., Degoulet, M., Risso, J.J. & Abraini, J.H. (2009). Post-ischemic helium provides neuroprotection in rats subjected to middle cerebral artery occlusion-induced ischemia by producing hypothermia. *J. Cereb. Blood Flow Metab.* Vol. 29 No. 6: pp. 1159-1165.

David, H.N., Haelewyn, B., Degoulet, M., Lecocq, M., Colomb, D.G. & Abraini, J.H. (submitted). Argon-induced neuroprotection in in-vivo models of ecitotoxic insult and ischemic brain damage in rats. *Br. J. Anaesth.*

David, H.N., Haelewyn, B., Risso, J.J., Colloc'h, N. & Abraini, J.H. (2010). Xenon is an inhibitor of tissue-plasminogen activator: adverse and beneficial effects in a rat model of thromboembolic stroke. *J. Cereb. Blood Flow Metab.* Vol. 30 No. 4: pp. 718-728.

David, H.N., Haelewyn, B., Rouillon, C., Lecoq, M., Chazalviel, L., Apiou, G., Risso, J.J., Lemaire, M. & Abraini, J.H. (2008). Neuroprotective effects of xenon: a therapeutic window of opportunity in rats subjected to transient cerebral ischemia. *Faseb J.* Vol. 22 No. 4: pp. 1275-1286.

David, H.N., Leveillé, F., Chazalviel, L., MacKenzie, E.T., Buisson, A., Lemaire, M. & Abraini, J.H. (2003). Reduction of ischemic brain damage by nitrous oxide and xenon. *J. Cereb. Blood Flow Metab.* Vol. 23 No. 10: pp. 1168-1173.

Demange, P., Voges, D., Benz, J., Liemann, S., Göttig, P., Berendes, R., Burger, A. & Huber, R. (1994). Annexin V: the key to understanding ion selectivity and voltage regulation? *Trends Biochem. Sci.* Vol. 19 No. 7: pp. 272-276.

Dingley, J., Tooley, J., Porter, H. & Thoresen, M. (2006). Xenon provides short-term neuroprotection in neonatal rats when administered after hypoxia-ischemia. *Stroke* Vol. 37 No. 2: pp. 501-506.

Dirnagl, U., Iadecola, C. & Moskowitz, M.A. (1999). Pathobiology of ischaemic stroke: an integrated view. *Trends Neurosci.* Vol. 22 No. 9: pp. 391-397.

Duff, A.P., Trambaiolo, D.M., Cohen, A.E., Ellis, P.J., Juda, G.A., Shepard, E.M., Langley, D.B., Dooley, D.M., Freeman, H.C. & Guss, J.M. (2004). Using xenon as a probe for dioxygen-binding sites in copper amine oxidases. *J. Mol. Biol.* Vol. 344 No. 3: pp. 599-607.

Dundas, J., Ouyang, Z., Tseng, J., Binkowski, A., Turpaz, Y. & Liang, J. (2006). CASTp: computed atlas of surface topography of proteins with structural and topographical mapping of functionally annotated residues. *Nucleic Acids Res.* Vol. 34 No. Web Server issue: pp. W116-118.

Eckenhoff, R.G. (2001). Promiscuous ligands and attractive cavities: how do the inhaled anesthetics work? *Mol. Interv.* Vol. 1 No. 5: pp. 258-268.

Emsley, P. & Cowtan, K. (2004). Coot: model-building tools for molecular graphics. *Acta Crystallogr.* Vol. D60 No. 12: pp. 2126-2132.

Ewing, J.G. & Maestas, S. (1970). Thermodynamics of absorption of xenon by myoglobin. *J. Phys. Chem.* Vol. 74 No. 11: pp. 2341-2344

Fourme, R., Girard, E., Kahn, R., Dhaussy, A.C., Mezouar, M., Colloc'h, N. & Ascone, I. (2006). High-pressure macromolecular crystallography (HPMX): status and prospects. *Biochim. Biophys. Acta* Vol. 1764 No. 3: pp. 384-390.

Franks, N.P. (2008). General anaesthesia: from molecular targets to neuronal pathways of sleep and arousal. *Nat. Rev. Neurosci.* Vol. 9 No. 5: pp. 370-386.

Franks, N.P., Dickinson, R., de Sousa, S.L., Hall, A.C. & Lieb, W.R. (1998). How does xenon produce anaesthesia? *Nature* Vol. 396 No. 6709: pp. 324.

Franks, N.P. & Lieb, W.R. (1984). Do general anaesthetics act by competitive binding to specific receptors ? *Nature* Vol. 310 No. 5978: pp. 599-601.

Franks, N.P. & Lieb, W.R. (1994). Molecular and cellular mechanisms of general anaesthesia. *Nature* Vol. 367 No. 6464: pp. 607-614.

Frauenfelder, H., Alberding, N.A., Ansari, A., Braunstein, D., Cowen, B.R., Hong, M.K., Iben, I.E.T., Johnson, J.B., Luck, S., Marden, M.C., Mourant, J.R., Ormos, P., reinisch, L., Scholl, R., Schiulte, A., Shyamsunder, E., Sorensen, L.B., Steinbach, P.J., Xie, A., Young, R.D. & Yue, K.T. (1990). Proteins and pressure. *J. Phys. Chem.* Vol. 94 No. 3: pp. 1024-1037.

Frauenfelder, H., Sligar, S.G. & Wolynes, P.G. (1991). The energy landscapes and motions of proteins. *Science* Vol. 254 No. 5038: pp. 1598-1603.

Girard, E., Marchal, S., Perez, J., Finet, S., Kahn, R., Fourme, R., Marassio, G., Dhaussy, A.C., Prangé, T., Giffard, M., Dulin, F., Bonneté, F., Lange, R., Abraini, J.H., Mezouar, M. & Colloc'h, N. (2010). Structure-function perturbation and dissociation of tetrameric urate oxidase by high hydrostatic pressure. *Biophys. J.* Vol. 98 No. 10: pp. 2365-2373.

Haelewyn, B., David, H.N., Colloc'h, N., Colomb, D.G., Risso, J.J. & Abraini, J.H. (2011). Interactions between nitrous oxide and tissue-plasminogen activator in a rat model of thromboembolic stroke. *Anesthesiol.* Vol. 115 No 5: pp. 1044-1053

Haelewyn, B., David, H.N., Rouillon, C., Chazalviel, L., Lecocq, M., Risso, J.J., Lemaire, M. & Abraini, J.H. (2008). Neuroprotection by nitrous oxide: facts and evidence. *Crit. Care Med.* Vol. 36 No. 9: pp. 2651-2659.

Homi, H.M., Yokoo, N., Ma, D., Warner, D.S., Franks, N.P., Maze, M. & Grocott, H.P. (2003). The neuroprotective effect of xenon administration during transient middle cerebral artery occlusion in mice. *Anesthesiol.* Vol. 99 No. 4: pp. 876-881.

Hubbard, S.J., Gross, K.H. & Argos, P. (1994). Intramolecular cavities in globular proteins. *Protein Eng.* Vol. 7 No. 5: pp. 613-626.

Imai, T., Hiraoka, R., Seto, T., Kovalenko, A. & Hirata, F. (2007). Three-dimensional distribution function theory for the prediction of protein-ligand binding sites and affinities: application to the binding of noble gases to hen egg-white lysozyme in aqueous solution. *J. Phys. Chem. B* Vol. 111 No. 39: pp. 11585-11591.

Jevtovic-Todorovic, V., Todorovic, S.M., Mennerick, S., Powell, S., Dikranian, K., Benshoff, N., Zorumski, C.F. & Olney, J.W. (1998). Nitrous oxide (laughing gas) is an NMDA antagonist, neuroprotectant and neurotoxin. *Nat. Med.* Vol. 4 No. 4: pp. 460-463.

Johansson, J.S., Manderson, G.A., Ramoni, R., Grolli, S. & Eckenhoff, R.G. (2005). Binding of the volatile general anesthetics halothane and isoflurane to a mammalian beta-barrel protein. *Febs J.* Vol. 272 No. 2: pp. 573-581.

Kabsch, W. (2010). XDS. *Acta Crystallogr.* Vol. D66 No. 2: pp. 125-132.

Kennedy, R.R., Stokes, J.W. & Downing, P. (1992). Anaesthesia and the 'inert' gases with special reference to xenon. *Anaesth. Intensive Care* Vol. 20 No. 1: pp. 66-70.

Kim, C.U., Hao, Q. & Gruner, S.M. (2007). High-pressure cryocooling for capillary sample cryoprotection and diffraction phasing at long wavelengths. *Acta Crystallogr.* Vol. D63 No. 5: pp. 653-659.

Koblin, D.D., Fang, Z., Eger, E.I., II, Laster, M.J., Gong, D., Ionescu, P., Halsey, M.J. & Trudell, J.R. (1998). Minimum alveolar concentrations of noble gases, nitrogen, and sulfur hexafluoride in rats: helium and neon as nonimmobilizers (nonanesthetics). *Anesth. Analg.* Vol. 87 No. 2: pp. 419-424.

Lee, J.M., Zipfel, G.J. & Choi, D.W. (1999). The changing landscape of ischaemic brain injury mechanisms. *Nature* Vol. 399 No. 6738 Suppl: pp. A7-14.

Leslie, A.G. (2006). The integration of macromolecular diffraction data. *Acta Crystallogr.* Vol. D62 No 1: pp. 48-57.

Li de la Sierra, I., Papamichael, E., Sakarellos, C., Dimicoli, J.L. & Prangé, T. (1990). Interaction of the peptide CF3-Leu-Ala-NH-C6H4-CF3 (TFLA) with porcine pancreatic elastase. X-ray studies at 1.8 A. *J. Mol. Recognit.* Vol. 3 No. 1: pp. 36-44.

Lo, E.H., Moskowitz, M.A. & Jacobs, T.P. (2005). Exciting, radical, suicidal: how brain cells die after stroke. *Stroke* Vol. 36 No. 2: pp. 189-192.

Luo, Y., Ma, D., Ieong, E., Sanders, R.D., Yu, B., Hossain, M. & Maze, M. (2008). Xenon and sevoflurane protect against brain injury in a neonatal asphyxia model. *Anesthesiol.* Vol. 109 No. 5: pp. 782-789.

Ma, D., Hossain, M., Chow, A., Arshad, M., Battson, R.M., Sanders, R.D., Mehmet, H., Edwards, A.D., Franks, N.P. & Maze, M. (2005). Xenon and hypothermia combine to provide neuroprotection from neonatal asphyxia. *Ann. Neurol.* Vol. 58 No. 2: pp. 182-193.

Ma, D., Yang, H., Lynch, J., Franks, N.P., Maze, M. & Grocott, H.P. (2003). Xenon attenuates cardiopulmonary bypass-induced neurologic and neurocognitive dysfunction in the rat. *Anesthesiol.* Vol. 98 No. 3: pp. 690-698.

Marassio, G., Prangé, T., David, H.N., Sopkova-de Oliveira Santos, J., Gabison, L., Delcroix, N., Abraini, J.H. & Colloc'h, N. (2011). Pressure-response analysis of anesthetic gases xenon and nitrous oxide on urate oxidase: a crystallographic study. *Faseb J.* Vol. 25 No. 7: pp. 2266-2275.

Miller, K.W. (2002). The nature of sites of general anaesthetic action. *Brit. J. Anaesthesia* Vol. 89 No. 1: pp. 17-31.

Mueller-Dieckmann, C., Polentarutti, M., Djinovic Carugo, K., Panjikar, S., Tucker, P.A. & Weiss, M.S. (2004). On the routine use of soft X-rays in macromolecular crystallography. Part II. Data-collection wavelength and scaling models. *Acta Crystallogr.* Vol. D60 No. 1: pp. 28-38.

Murshudov, G.N., Vagin, A.A. & Dodson, E.J. (1997). Refinement of macromolecular structures by the Maximum-Likelihood method. *Acta Crystallogr.* Vol. D53: pp. 240-255.

NINDS (1995). Tissue plasminogen activator for acute ischemic stroke. The National Institute of Neurological Disorders and Stroke rt-PA Stroke Study Group. *N. Engl. J. Med.* Vol. 333 No. 24: pp. 1581-1587.

Olney, J.W., Labruyere, J., Wang, G., Wozniak, D.F., Price, M.T. & Sesma, M.A. (1991). NMDA antagonist neurotoxicity: mechanism and prevention. *Science* Vol. 254 No. 5037: pp. 1515-1518.

Otwinowski, Z. & Minor, W. (1997). Processing of X-ray diffraction data collected in the oscillation mode. *Methods Enzymol.* Vol. 276: pp. 307-326.

Panjikar, S. & Tucker, P.A. (2002). Xenon derivatization of halide-soaked protein crystals. *Acta Crystallogr.* Vol. D58 No. 9: pp. 1413-1420.

Prangé, T., Schiltz, M., Pernot, L., Colloc'h, N., Longhi, S., Bourguet, W. & Fourme, R. (1998). Exploring hydrophobic sites in proteins with xenon or krypton. *Proteins* Vol. 30 No. 1: pp. 61-73.

Quillin, M.L., Breyer, W.A., Griswold, I.J. & Matthews, B.W. (2000). Size *versus* polarizability in protein-ligand interactions: binding of noble gases within engineered cavities in phage T4 lysozyme. *J. Mol. Biol.* Vol. 302 No. 4: pp. 955-977.

Russell, G.B. & Graybeal, J.M. (1992). Direct measurement of nitrous oxide MAC and neurologic monitoring in rats during anesthesia under hyperbaric conditions. *Anesth. Analg.* Vol. 75 No. 6: pp. 995-999.

Ruzicka, J., Benes, J., Bolek, L. & Markvartova, V. (2007). Biological effects of noble gases. *Physiol. Res.* Vol. 56 No. Suppl 1: pp. S39-44.

Sanders, R.D., Ma, D. & Maze, M. (2004). Xenon: elemental anaesthesia in clinical practice. *Br. Med. Bull.* Vol. 71: pp. 115-135.

Sanders, R.D. & Maze, M. (2005). Xenon: from stranger to guardian. *Curr. Opin. Anaesthesiol.* Vol. 18 No. 4: pp. 405-411.

Schiltz, M., Fourme, R., Broutin, I. & Prangé, T. (1995). The catalytic site of serine proteinases as a specific binding cavity for xenon. *Structure* Vol. 3 No. 3: pp. 309-316.

Schiltz, M., Fourme, R. & Prangé, T. (2003). Use of noble gases xenon and krypton as heavy atoms in protein structure determination. *Methods Enzymol.* Vol. 374: pp. 83-119.

Schiltz, M., Prangé, T. & Fourme, R. (1994). On the preparation and X-ray data collection of isomorphous xenon derivatives. *J. Appl. Crystallogr.* Vol. 27: pp. 950-960.

Schiltz, M., Shepard, W., Fourme, R., Prangé, T., de la Fortelle, E. & Bricogne, G. (1997). High-pressure krypton gas and statistical heavy-atom refinement: a successful combination of tools for macromolecular structure determination. *Acta Crystallogr.* Vol. D53 No. 1: pp. 78-92.

Schoenborn, B.P. (1965). Binding of xenon to horse haemoglobin. *Nature* Vol. 208 No. 5012: pp. 760-762.

Schoenborn, B.P., Watson, H.C. & Kendrew, J.C. (1965). Binding of xenon to sperm whale myoglobin. *Nature* Vol. 207 No. 992: pp. 28-30.

Takeda, K., Miyatake, H., Park, S.Y., Kawamoto, M., Kamiya, N. & Miki, K. (2004). Multi-wavelength anomalous diffraction method for I and Xe atoms using ultra-high-energy X-rays from SPring-8. *J. Appl. Crystallogr.* Vol. 37: pp. 925-933.

Tilton, R.F., Jr., Kuntz, I.D., Jr. & Petsko, G.A. (1984). Cavities in proteins: structure of a metmyoglobin-xenon complex solved to 1.9 Å. *Biochemistry* Vol. 23 No. 13: pp. 2849-2857.

Trudell, J.R. (1977). A unitary theory of anesthesia based on lateral phase separations in nerve membranes [proceedings]. *Biophys. J.* Vol. 18 No. 3: pp. 358-359.

Vitali, J., Robbins, A.H., Almo, S.C. & Tilton, R.F. (1991). Using xenon as a heavy atom for determining phases in sperm whale met-myoglobin. *J. Appl. Crystallogr.* Vol. 24 No. 5: pp. 931-935.

Yamakura, T. & Harris, R.A. (2000). Effects of gaseous anesthetics nitrous oxide and xenon on ligand-gated ion channels. Comparison with isoflurane and ethanol. *Anesthesiol.* Vol. 93 No. 4: pp. 1095-1101.

IntechOpen

IntechOpen

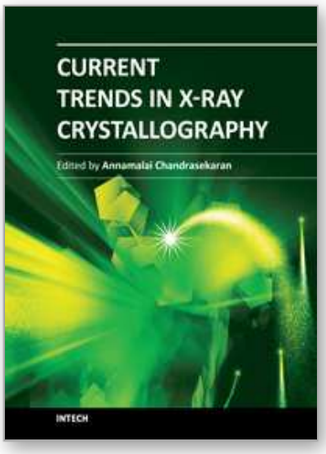

Current Trends in X-Ray Crystallography

Edited by Dr. Annamalai Chandrasekaran

ISBN 978-953-307-754-3

Hard cover, 436 pages

Publisher InTech

Published online 16, December, 2011

Published in print edition December, 2011

This book on X-ray Crystallography is a compilation of current trends in the use of X-ray crystallography and related structural determination methods in various fields. The methods covered here include single crystal small-molecule X-ray crystallography, macromolecular (protein) single crystal X-ray crystallography, and scattering and spectroscopic complimentary methods. The fields range from simple organic compounds, metal complexes to proteins, and also cover the meta-analyses of the database for weak interactions.

How to reference

In order to correctly reference this scholarly work, feel free to copy and paste the following:

Nathalie Colloc'h, Guillaume Marassio and Thierry Prange (2011). Protein-Noble Gas Interactions Investigated by Crystallography on Three Enzymes - Implication on Anesthesia and Neuroprotection Mechanisms, Current Trends in X-Ray Crystallography, Dr. Annamalai Chandrasekaran (Ed.), ISBN: 978-953-307-754-3, InTech, Available from: http://www.intechopen.com/books/current-trends-in-x-ray-crystallography/protein-noble-gas-interactions-investigated-by-crystallography-on-three-enzymes-implication-on-anest

INTECH
open science | open minds

InTech Europe
University Campus STeP Ri
Slavka Krautzeka 83/A
51000 Rijeka, Croatia
Phone: +385 (51) 770 447
Fax: +385 (51) 686 166
www.intechopen.com

InTech China
Unit 405, Office Block, Hotel Equatorial Shanghai
No.65, Yan An Road (West), Shanghai, 200040, China
中国上海市延安西路65号上海国际贵都大饭店办公楼405单元
Phone: +86-21-62489820
Fax: +86-21-62489821

© 2011 The Author(s). Licensee IntechOpen. This is an open access article distributed under the terms of the Creative Commons Attribution 3.0 License, which permits unrestricted use, distribution, and reproduction in any medium, provided the original work is properly cited.